Modeling Square-Wave Voltammetry of Thin Protein Films Using Marcus Theory

Trevor M. Saccucci and James F. Rusling*

Department of Chemistry, The University of Connecticut, U-60, Storrs, Connecticut 06269-3060

Received: October 4, 2000; In Final Form: April 18, 2001

A model combining Marcus theory with Gaussian distributions of kinetic and thermodynamic parameters was developed for square-wave voltammetry (SWV) and applied to the protein myoglobin in thin films of didodecyldimethylammonium bromide on electrodes. Nonlinear regression analysis allowed direct estimation of electron transfer rate constants and reorganization energies from single experiments at relatively large pulse heights. Successful fitting relies on the accurate representation of background current within the model. Analysis of 22 voltammograms at pH 6 over a range of frequencies and pulse heights gave a formal potential consistent with earlier determinations, and a mean $\log(k_{RED}^{null})$ of $3.3 + 0.8\ s^{-1}$, not significantly different from the mean $\log(k_{OX}^{null})$ of $3.0 \pm 0.6\ s^{-1}$. The mean value of reorganization energy λ_{RED} was 0.41 ± 0.02 eV and λ_{OX} was 0.21 ± 0.01 eV. Differences in λ_{RED} and λ_{OX} are likely to reflect different solvation, bonding, and conformation near the iron heme regions of $MbFe^{III}$ and $MbFe^{II}$. Methods presented here promise to be generally applicable to determining Marcus electron-transfer parameters for redox proteins in thin films.

Introduction

Measuring kinetic and thermodynamic parameters for electron transfer of redox proteins is important for a fundamental understanding of biological electron transfer, as well as for the development of effective bioreactors and biosensors. Protein film voltammetry provides a straightforward approach to this task.[1] Thin films of insoluble surfactants can be used to confine redox proteins in environments similar to those of the biological membranes they are often bound to in living systems. When diffusion of the proteins within these films is fast on the time scale of the experiment, the kinetic analysis of voltammetric data may be simplified by the elimination of diffusion effects.[1−4] However, electroactive protein films typically exhibit nonideal thin-film electrochemical behavior. Approaches to dealing with this fact have involved modeling electrochemical responses of these systems using dispersions of kinetic and thermodynamic parameters.[2,3,5] Dispersion in formal potentials and/or rate constants has been used to account for peak broadening in voltammetry and nonlinear $\log(i)-t$ plots in chronoamperometry.[3,5,6−8]

Thin films of surfactant bilayers containing redox proteins such as myoglobin, hemoglobin, and cytochrome P450s can be viewed as models of natural systems where proteins are bound onto or within cell membranes in living cells.[1b] We studied the mammalian oxygen-transport protein myoglobin (Mb) incorporated into thin films of didodecyldimethylammonium bromide (DDAB), lipids, and other surfactants on the surfaces of basal plane pyrolytic graphite (PG) electrodes.[1b,3] Mb in these films exhibits chemically reversible electron exchange with the electrode, uncomplicated by coupled chemical reactions on typical voltammetric time scales. Mb physically diffuses within DDAB films. Electrochemical kinetics of Mb−DDAB and other film systems were previously treated using the Butler−Volmer theory of electrode kinetics,[9] which pertains when the applied overpotential, η, is much smaller than the reorganization energy, λ, of the heterogeneous electron-transfer reaction. Here, λ is the sum of terms for inner-sphere reorganization energy, due to bonding within the redox center, and outer-sphere reorganization energy, due to solvation.[8,10]

The outer-sphere component of λ decreases with decreasing dielectric constant of the medium.[8,10] ESR anisotropy, visible linear dichroism spectroscopy,[11] and atomic force microscopy[12] studies suggest that Mb in surfactant films resides mainly in a hydrophobic environment. Thus, the environment surrounding the Mb in the film would have a relatively low dielectric constant. This would result in λ not being much larger than η.

We previously reported a model for nonlinear regression (NLR) analysis of thin-layer square-wave voltammetry (SWV) to determine electron-transfer parameters in protein films using Butler−Volmer theory with dispersion in $E^{0\prime}$ values.[3] SWV was used because of its better signal-to-noise ratio than that of cyclic voltammetry and because of the availability of closed form expressions for the current.[13] The general Marcus theory of electron transfer, of which Butler−Volmer is a special case, best describes the electron-transfer kinetics of redox centers in systems where λ is not much larger than η.[2,5c−d,8,10,14,15]

In this paper, we describe a model employing Marcus theory to describe the electron-transfer kinetics and dispersion in all thermodynamic and kinetic parameters. We also consider the possibility of nonequivalent kinetic parameters for oxidations and reductions.[16] We report herein the first use, to our knowledge, of regression analysis of SWV to determine electron-transfer activation parameters for a protein in a thin film using Marcus theory. Mb−DDAB films on ordinary pyrolytic graphite electrodes serve as the experimental system.

Experimental Section

Materials. Myoglobin (Mb) (Sigma) from horse skeletal muscle was purified as described previously.[3] The electrolyte was pH 6.0 buffer of 20 mM ionic strength sodium potassium acid phthalate (NaKHP) and 180 mM NaCl. Didodecyldimethylammonium bromide (DDAB) (>99%) was from Acros. Water had specific resistance ≥18 MΩ cm.

Apparatus and Procedures. Methods for square-wave voltammetry were described previously,[3] and a CH Instruments

* Corresponding author.

10.1021/jp0036339 CCC: $20.00
Published on Web 06/07/2001

Model 660a Electrochemical Workstation was employed. The reference electrode was a saturated calomel electrode (SCE), and the counter electrode was a Pt coil. Working electrodes were ordinary basal plane pyrolytic graphite disks (PG, $A = 0.016$ cm^2, Advanced Ceramics) prepared and coated with Mb−DDAB films as described previously.[3] The cell resistance was 35−40 Ω and was electronically compensated to 10−14 Ω uncompensated resistance. The temperature was 37.0 ± 0.2 °C. At this temperature, pH, and ionic strength, Mb is in its native conformation.[3,11,17] Kinetic parameters were obtained through nonlinear regression analysis[18] of SWV data onto the model below.

Overview of the Model. All programming was done using Matlab 5.2 with the Optimization Toolbox. The total current is computed as a linear function of the generally nonlinear functions describing the main electron-transfer reaction and the background processes. In matrix form

$$\mathbf{I} = \mathbf{\Phi}\boldsymbol{\beta} \tag{1}$$

where **I** is the column vector containing the total computed current from all processes, **Φ** is a matrix with each column containing the product of a normalized dimensionless current function and a dimensioned scalar constant, and $\boldsymbol{\beta}$ is a column vector of dimensionless linear scale factors determined from multiple linear regression. The matrix of normalized dimensionless current functions $\hat{\boldsymbol{\psi}}$ is

$$\hat{\boldsymbol{\psi}} = [\boldsymbol{\psi}_{\mathrm{MAX}}{}^{-1}\boldsymbol{\psi}] \tag{2}$$

where $\boldsymbol{\psi}$ is a matrix with columns containing the current function for the main electron-transfer process of interest and an arbitrary number of background processes and $\boldsymbol{\psi}_{\mathbf{MAX}}{}^{-1}$ is a diagonal matrix with each nonzero entry containing the reciprocal of the maximum absolute value of its corresponding column in $\boldsymbol{\psi}$. **Φ** is given by

$$\mathbf{\Phi} = \hat{\mathbf{A}}\hat{\boldsymbol{\psi}} \tag{3}$$

where **B** is a diagonal matrix with each nonzero entry containing a dimensioned, algebraically signed constant scale factor entered by the user. The user-estimated dimensioned current from the process corresponding to the *l*th column of $\hat{\boldsymbol{\psi}}$ is

$$\mathbf{\Phi}_l = \hat{A}_{\mathrm{ll}}\hat{\boldsymbol{\psi}}_{\mathrm{l}} \tag{4}$$

where the algebraic sign of each $\hat{A}^{\mathrm{ll}}$ is provided by the algebraic sign flag for its corresponding current, which has a value of +1 for reductions and −1 for oxidations.

Data analysis employs the Marquardt−Levenberg nonlinear regression algorithm to optimize the shape of the model current.[19] The shape functions are normalized to a maximum absolute value of unity and scaled inside the Marquardt−Levenberg routine to form **Φ**, and a multiple linear regression routine is used to regress the experimental square-wave voltammetry data onto **Φ** to form **I**. Following the suggestion of Borse,[20] the objective function χ^2 for the nonlinear regression routine is then formed as

$$\chi^2 = \boldsymbol{W}^T\boldsymbol{W} \tag{5}$$

where $\boldsymbol{W}$ is a column vector with as many entries as data points, with each entry $\boldsymbol{W}_s$ given by

$$\boldsymbol{W}_s = \frac{(1 + \upsilon\hat{\boldsymbol{\psi}}_{\mathrm{m,s}})(i_{\mathrm{meas},s} - I_s)}{\Delta i_{\mathrm{meas}}} \tag{6}$$

Here, $i_{\mathrm{meas},s}$ is the *s*th entry in a column vector containing the measured experimental square-wave current; I_s, is the *s*th entry in the model current vector **I**, $\hat{\boldsymbol{\psi}}_{\mathrm{m,s}}$ is the *s*th entry in the normalized dimensionless current function for the main electron-transfer reaction being modeled, υ is a user-selected constant, and Δi_{meas} is the user-estimated per point standard deviation of the experimental current, assumed to be the same for all data points. The $(1 + \upsilon\hat{\boldsymbol{\psi}}_{m,s})$ term in eq 5 above is a weighting factor which was chosen to ensure that SWV peaks from the main redox reaction would be fitted using the Marcus model, and not the model used for the background currents. A value of $\upsilon = 2$, chosen by trial and error, was used in all of the SWV analyses in this work.

Modeling SWV with Marcus Theory. Each parameter in the model was represented by a Gaussian distribution uniquely defined by two model parameters representing the end points of the dispersion of values for each parameter. End points 5 standard deviations on either side of the mean were used. The resulting dispersion of electrochemical responses was modeled as a normal Gaussian divided into *p* segments and integrated segment-by-segment as the regression runs. The total square-wave current is then given by

$$\mathbf{i} = \sum_{j=1}^{p}\mathbf{i}_j \tag{7}$$

where $\mathbf{i}_j$ is the contribution of the *j*th population of redox centers to the total current, given by

$$\mathbf{i}_j = \boldsymbol{\beta}_{\mathbf{MAIN}}\mathbf{B}_{\mathbf{MAIN}}\mathbf{A}_j\boldsymbol{\psi}_j \tag{8}$$

Here, $\mathbf{A}_j$ is the area of the *j*th segment of the integrated normal Gaussian curve, $\boldsymbol{\beta}_{\mathbf{MAIN}}$ and $\mathbf{B}_{\mathbf{MAIN}}$ are the entries in $\boldsymbol{\beta}$ and **B** corresponding to the main ET reaction, and the dimensionless current function for the main ET reaction, $\boldsymbol{\psi}_j$, is given by

$$\boldsymbol{\psi}_j = [(\kappa_{\mathrm{f},j} + \kappa_{\mathrm{b},j})\mathbf{\Gamma}'_{0,j} - \kappa_{\mathrm{b},j}]\exp[-(\kappa_{\mathrm{f},j} + \kappa_{\mathrm{b},j})] \tag{9}$$

where $\mathbf{\Gamma}'_{0,j}$ is the dimensionless surface concentration of the *j*th

$$\mathbf{\Gamma}''_{0,j} = (\mathbf{\Psi}_j + \kappa_{\mathrm{b},j})/(\kappa_{\mathrm{f},j} + \kappa_{\mathrm{b},j}) \tag{10}$$

population at time $t = 0$ and $\mathbf{\Gamma}''_{0,j}$ is the dimensionless surface concentration at $t = t_{\mathrm{p}}$, the square-wave pulse time. $\mathbf{\Gamma}'_{0,j}$ is always equal to unity. The dimensionless rate parameter $\kappa_{\mathrm{f},j} = k_{\mathrm{f},j}t_{\mathrm{p}}$, and $\kappa_{\mathrm{b},j} = k_{\mathrm{b},j}t_{\mathrm{p}}$. The first-order rate constants for the *j*th population of redox centers are computed from Marcus theory for heterogeneous ET as stated by Nahir and Bowden[5c,d]

$$\mathbf{k}_{\mathrm{RED},j} = k^{\mathrm{null}}_{\mathrm{RED},j}\left(1 + erf\left(\frac{(\eta_j + \lambda_{\mathrm{RED},j})F}{(\sqrt{4}\lambda_{\mathrm{RED},j}FRT)}\right)\right) \tag{11}$$

$$\mathbf{k}_{\mathrm{OX},j} = k^{\mathrm{null}}_{\mathrm{OX},j}\,erfc\left(\frac{(\eta_j + \lambda_{\mathrm{OX},j})F}{(\sqrt{4}\lambda_{\mathrm{OX},j}FRT)}\right) \tag{12}$$

where $\lambda_{\mathrm{RED},j}$ and $\lambda_{\mathrm{OX},j}$ are reorganization energies for reduction and oxidation, respectively, and $\lambda^{\mathrm{null}}_{\mathrm{RED},j}$ and $\lambda^{\mathrm{null}}_{\mathrm{OX},j}$ (s^{-1}) are first-order heterogeneous electron-transfer rate constants when $\eta_j + \lambda_{\mathrm{RED},j}$ and $\eta_j + \lambda_{\mathrm{OX},j}$, respectively, are equal to zero. η_j is the overpotential

$$\eta_j = E - E_j^{0'} \tag{13}$$

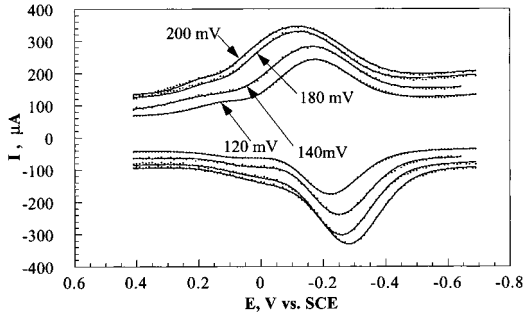

Figure 1. Forward and reverse square-wave voltammograms of Mb−DDAB films on PG electrodes at 200 Hz frequency, 10 mV step height, and different pulse heights. Points are experimental data, and lines are best fits by nonlinear regression onto the Marcus model. Background currents are included in experimental and computed data. $T = 37.0 \pm 0.2$ °C, and the supporting electrolyte is 20 mM pH 6.0 phthalate buffer + 180 mM NaCl.

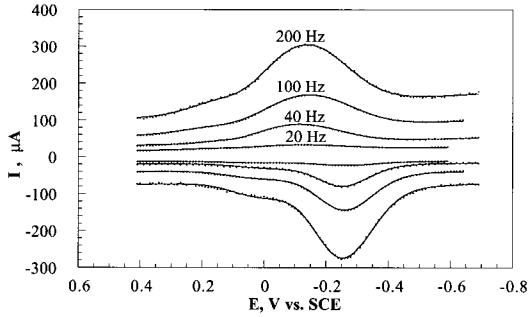

Figure 2. Forward and reverse square-wave voltammograms of Mb−DDAB films on PG electrodes at 160 mV pulse height, 10 mV step height, and different frequencies. Points are experimental data, and lines are best fits by nonlinear regression onto the Marcus model. Background currents are included in experimental and computed data. $T = 37.0 \pm 0.2$ °C, and the supporting electrolyte is 20 mM pH 6.0 phthalate buffer + 180 mM NaCl.

where $E_j^{0'}$ is the formal potential of the redox centers and E is the applied potential. F is Faraday's constant, R is the universal gas constant, and T is the absolute temperature. For the reduction of Mb, k_f and k_b are rate constants for reduction and oxidation, respectively.

The nonlinear model for the main ET reaction was parametrized as high and low distribution end point values of log (κ_{RED}^{null}), log(κ_{OX}^{null}), log(λ_{RED}/eV), log(λ_{OX}/eV), and $E_j^{0'}$ where $\kappa_{RED}^{null} = k_{RED}^{null}\, t_p$ and $\kappa_{OX}^{null} = k_{OX}^{null}\, t_p$. The number of populations p is parametrized as log(p). The actual distributions in the model are Gaussian in log(κ_{RED}^{null}) and log(κ_{OX}^{null}), λ_{RED} and λ_{OX}, and $E_j^{0'}$. Accurate representation of background current was essential for the success of the fitting. Details are included as Supporting Information.

The parameters determined by nonlinear regression analyses showed no significant correlations,[18] except occasional partial correlation where the model parameters represented the end points of the distribution of a single electrochemical parameter. This occurred when the end points had similar values, indicating only that there was a small dispersion in that parameter, not that the parametrization was flawed.

Results

Square-Wave Voltammetry of Mb−DDAB Films. Mb−DDAB films of the thickness used in this work (ca. 0.5 μm) exhibit nonideal thin-layer SWV behavior, but with peak current proportional to frequency at up to at least 240 Hz.[3] Twenty-two SWVs of Mb−DDAB films were analyzed at frequencies of 20−200 Hz and pulse heights 100−200 mV. Preliminary computations with noisy theoretical data showed that these relatively high pulse heights were necessary to achieve good precision in determining λ values. Excellent fits of the model to SWV data were obtained (Figures 1 and 2). Asymmetry in forward and reverse peaks became apparent with increasing pulse height (Figure 1). This is expected if rate constants κ_{RED}^{null} and κ_{OX}^{null} and/or the reorganization energies λ_{RED} and λ_{OX} are significantly different from each other. Figure 2 shows the effect of changing square-wave frequency at a constant pulse height.

An example of the computed Gaussian dispersion in a single electrochemical parameter is shown in Figure 3 for $E^{0\prime}$. Each bar in the histogram corresponds to a single voltammetric response computed from a single set of electrochemical parameters taken from one population of the dispersion. The effect of dispersion in electrochemical parameters on the net rate constant $(\kappa_{RED} + \kappa_{OX})$ is shown in Figure 4. Each curve in Figure 4 represents a set of net rate constant versus overpotential

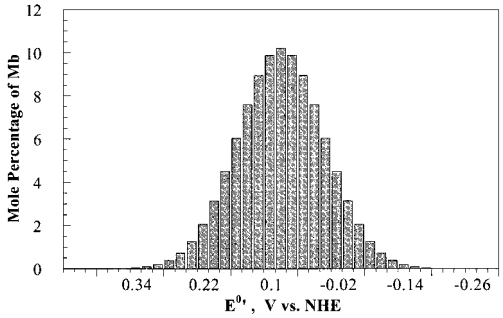

Figure 3. Histogram showing mole percentage of Mb in a film vs $E^{0\prime}$ from regression analysis of SWV data at 200 Hz frequency; 160 mV pulse height from Figure 2. Thirty-nine populations are represented.

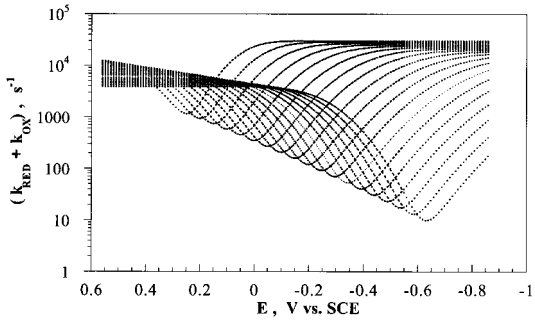

Figure 4. Influence of overpotential on the estimated $k_{RED} + k_{OX}$ for representative populations in the Gaussian distribution from regression analysis of SWV data at 200 Hz frequency; 160 mV pulse height from Figure 2. Every other curve is shown for clarity.

data computed for a single population of dispersed parameters. Note that the curves flatten out at high overpotentials, which is exactly the prediction from Marcus theory. This is also demonstrated in calculated model log $(\kappa_{RED} + \kappa_{OX})$ versus overpotential at small λ (Figure 5). At the highest k shown, the curve tends toward an exponential increase in rate constant with overpotential, as predicted by Butler−Volmer theory.[8,10,14,15]

Bump-like distortions in peak shapes in Figures 1 and 2 are the result of background processes associated with the carbon electrode. When the fitted background current is subtracted from experimental voltammograms, a perfectly regular SWV is obtained with no evident distortions or background (Figure 6) and a good match of baselines on the forward and reverse SWVs. Goodness of fit is also supported by the of the residuals from the regression analysis in Figure 7, with little patterning evident suggesting an excellent fit of the background-subtracted

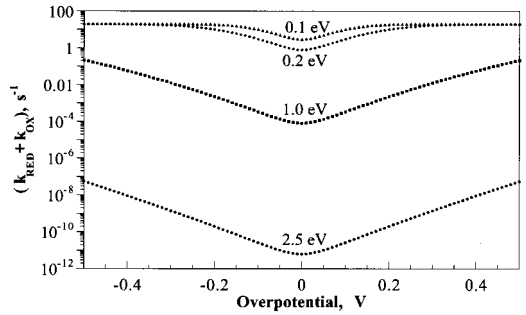

Figure 5. Influence of overpotential on $k_{RED} + k_{OX}$ calculated for different values of recognization energy. Conditions used in the calculation were $T = 25.0$ °C, pulse width = 1 s, $k^{null}_{RED/OX} = 10$ s^{-1}, $\lambda_{RED} = \lambda_{OX}$, and $E^{0\prime} = 0$ V.

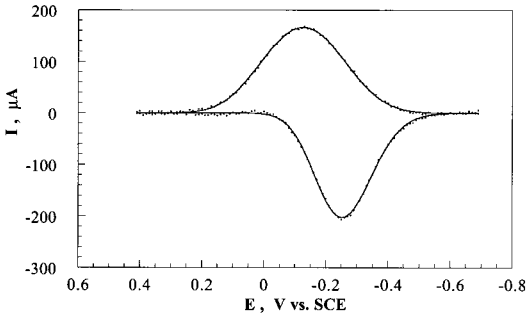

Figure 6. Experimental currents (points) with model background currents subtracted, resulting from regression analysis of SWV data at 200 Hz frequency; 160 mV pulse height data shown in Figure 2. Solid line represents computed result.

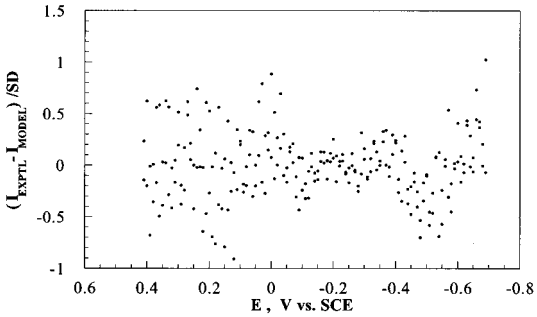

Figure 7. Deviation plot of residuals for experimental and calculated data from regression analysis of SWV data at 200 Hz frequency; 160 mV pulse height data shown in Figure 2.

data to the model.[18] A chi-square analysis of this plot gave a 100% probability that the errors were normally distributed, with the standard deviation of the experimental data estimated at 2% of the maximum current. This estimate may be somewhat high, as evidenced by a maximum excursion from zero of approximately one standard deviation in Figure 7. Nevertheless, these data are typical and illustrate the reliability of the background fitting.

Figure 8 shows the means of the Gaussian distributions of $\log(\kappa^{null}_{RED})$ and $\log(\kappa^{null}_{OX})$ from nonlinear regression analyses of SWV. Values show a slight increasing trend with increasing SWV frequency (i.e., decreasing pulse width) but are essentially independent of pulse height below 100 Hz. Interestingly, for mean first-order electron transfer, rate constants on semiconductor electrodes shifted from lower to higher values as the observation time window decreased,[7] similar to our observations. This is attributed to the influence of the observation time on dispersed decay kinetics. In SWV, net exponential decay current is measured at the end of each potential pulse. At shorter

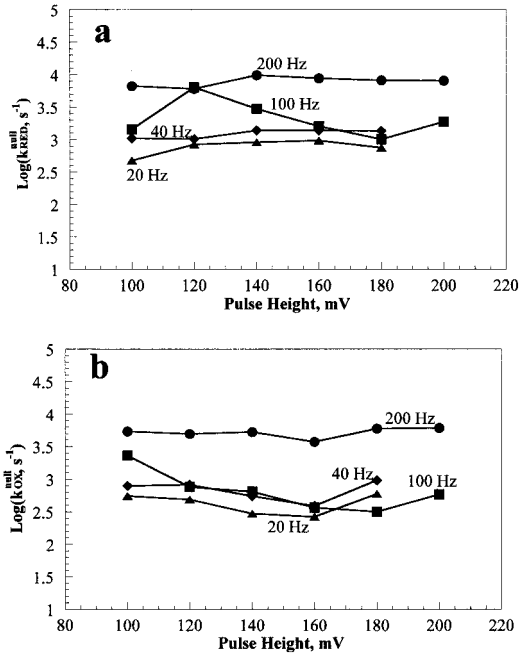

Figure 8. Influence of square-wave pulse height on mean values of $\log(k^{null}_j/s^{-1})$ from regression analyses of SWV data taken at 20−200 Hz frequency and 100−200 mV pulse height. (a) j = RED; (b) j = OX.

TABLE 1: Pooled Mean Parameters for Myoglobin in a DDAB Films from Regression Analysis of SWV Data[a]

pooled mean	value ± s.d.
$\log(k^{null}_{RED}/s^{-1})$	3.3 ± 0.8
$\log(k^{null}_{OX}/s^{-1})$	3.0 ± 0.6
λ_{RED}/eV	0.41 ± 0.02
λ_{OX}/eV	0.21 ± 0.01
$E^{0\prime}$/V vs NHE	0.082 ± 0.021

[a] Values are pooled from 22 voltammograms. Errors in parameters are given as standard deviations. Frequencies were 20, 40, 100, and 200 Hz. Step height was 10 mV. Pulse heights were 100, 120, 140, 160, 180, and 200 mV at 100 and 200 Hz, up to 180 mV only for 20 and 40 Hz. Experiments at 37.0 ± 0.2 °C.

measurement times, i.e., higher square-wave frequencies, components of the distribution with slower kinetics will not have begun to contribute, while those components with faster kinetics will predominate. At longer measurement times, i.e., lower square-wave frequencies, slower-decaying component currents will predominate, while fast-decaying components will contribute less.

The results in Table 1 are the pooled mean values of the means of the Gaussian distributions of parameters found by regression analysis. The $E^{0\prime}$ value of 0.082 ± 0.021 V versus NHE at pH 6 is in good agreement with 0.061 V versus NHE reported previously for Mb−DDAB films on PG electrodes.[3b] The $\log(\kappa^{null}_{RED})$ of 3.3 ± 0.8 s^{-1} is not significantly different from the $\log(\kappa^{null}_{OX})$ of 3.0 ± 0.6 s^{-1}. κ^{null}_{RED} and κ^{null}_{OX} are proportional to $\exp(-d_{ET}/nm)$,[2,5c−d,8,10,14] where d_{ET} (nm) is the tunneling distance for electron transfer, so their similarity suggests no changes in average electron-transfer distance for Mb upon changing oxidation state. This is reasonable since Mb is mobile in DDAB films on the SWV time scale,[1b] and the average electron transfer distance probably reflects a "distance of closest approach" of the protein molecule in the film to the electrode−film interface.

The mean value of λ_{RED} of 0.41 ± 0.02 eV is very different from that of λ_{OX} at 0.21 ± 0.01 eV. The Fe^{III} and Fe^{II} forms of Mb and hemoglobin in solution have differences in secondary structure around the iron hemes,[21] and conformational differences between different redox states of cytochrome *c* (cyt *c*)[22] and other proteins[23] have also been clearly demonstrated. The difference in λ_{RED} and λ_{OX} is consistent with a change in protein structure and/or solvation around the Mb heme upon changing oxidation state, causing the reorganization energy barrier for oxidation of $MbFe^{II}$ to be lower than that for reduction of $MbFe^{III}$.

Discussion

Reorganization Energy of Mb. Marcus theory has been tested for electron-transfer involving Mb in several systems. λ values of 3.1 and 1.3 eV, respectively, were reported for electron transfer between photoexcited oxyferryl horse heart Mb and Zn-substituted sperm whale Mb in aqueous solution with covalently attached pentaammineruthenium.[24] λ between 1.90 and 2.45 eV was found for reaction between photoexcited Pd−(mesoporphyrin IX) substituted sperm whale Mb and covalently attached pentaammine ruthenium and trans-tetraammineruthenium.[25] Experimental λ values for electron transfer between Mb, cyt *c*, and cytochrome *b*5 (cyt *b*5) with attached Ru-containing cofactors agreed well with values calculated using the linear Poisson−Boltzmann equation.[26] They estimated an upper limit of 1.6 eV for reorganization energies of the proteins. These λ values reflect bimolecular redox reactions for chemically modified Mb in water. Since these reactions involve electron transfer between a natural and an unnatural redox center, the determination of a λ for each center is not possible without prior information about the reorganization energy of one of the reaction partners. Also, many redox proteins, such as the cytochromes P450 (cyt P450)[27] and cyt *c* oxidase, exist bound to membranes in mammalian cells where λ may be very different than that in water. Finally, individual values of λ_{RED} and λ_{OX} were not considered in the above studies.

The outer-sphere component of reorganization energy, shown in eq 14 for heterogeneous electron transfer, varies with the dielectric constants of the medium[8,10]

$$\lambda_{OS} = \frac{e^2 N}{8\pi\epsilon_0}\left(\frac{1}{a} - \frac{1}{2d}\right)\left(\frac{1}{\epsilon_{op}} - \frac{1}{\epsilon_s}\right) \qquad (14)$$

where *a* is the radius of the redox center, *d* is its normal distance from the surface of the electrode, ϵ_{op} and ϵ_s are the optical and static dielectric constants, respectively, of the medium surrounding the redox center, ϵ_0 is the permittivity of free space, *e* is the charge of a single electron, and net dielectric constant ϵ is given by[28]

$$\epsilon = \epsilon_o + \epsilon_s \qquad (15)$$

The $(1/\epsilon_{op} - 1/\epsilon_s)$ term in eq 14 is common to heterogeneous and homogeneous expressions for λ_{OS}. In the limit of a nonpolar medium, $\epsilon_{op} \simeq \epsilon_s$ and λ_{OS} tends toward zero. Mb in DDAB films resides in a relatively hydrophobic environment,[11] and the polarity of the medium around the protein in these films should be much less than that of bulk water. This may be the main reason that λ values in the DDAB films are smaller than those estimated for modified Mb's in water. Comparison can be made with electrochemical impedance and linear sweep voltammetry studies of Bowden and co-workers on cytochrome *c* electrostatically bound to a carboxyalkylthiol self-assembled monolayer (SAM) on gold electrodes.[5c,d] Using a model on which eqs 10 and 11 were based, they report a λ of 0.28 eV for cyt *c*[5d] as a lower limit in this film medium, which is at least partly hydrophobic. λ and the potential independent rate constant $k_{\eta,0}$ were assumed to have the same values for the different oxidation states of the protein.

Marcus theory has also been used to describe voltammetry and chronoamperometry of self-assembled monolayers of thioalkyl ferrocenes,[8,15] thioalkyl ruthenium-amine complexes,[29] and osmium bipyridyl complexes.[30] In these cases, λ and $k_{\eta,0}$ were assumed to be the same for oxidized and reduced forms.

Hupp and Weaver[16a] discussed implications of different values for λ_{RED} and λ_{OX} and found grossly asymmetric Tafel plots for the electrolysis of $Cr(OH_2)_6^{3+/2+}$ at mercury electrodes in aqueous solution, which they ascribed chiefly to differences in the inner-sphere coordination of the Cr, resulting in larger force constants for the $Cr-OH_2$ bond in the oxidized form than in the reduced form. From known structural parameters of the complex, they calculated λ_{RED} 3.21 eV and λ_{OX} 2.04 eV. They suggest that electron transfer reactions with coupled chemical reactions should have significantly different λ's for oxidation and reduction. They specifically cite the case of ET coupled to proton transfer as a signal example of this behavior. Significantly, Mb electron transfer in DDAB films is coupled to a fast preceding protonation.[3b] King et al.[31] reported the dissociation of a water molecule from the $MbFe^{II}$ center following its formation by reduction of $MbFe^{III}$ in solution, but we find no evidence for this in voltammetry of Mb−DDAB films.

Hoffman and Ratner[16b] treated the general case of unequal values for λ_{RED} and λ_{OX} in their discussion of the theoretical implications of internal bonding and solvent cage reorganization kinetics on the overall kinetics of homogeneous electron-transfer reactions of redox proteins. Hirst and Armstrong[2] ascribe the appearance of an extra peak and a shoulder in the cyclic voltammetry of thin films of several ferredoxin proteins at scan rates of 100 V s^{-1} and higher to measurable reorganization kinetics. We have not observed such behavior in our work with protein films. We therefore assume the reorganization kinetics are fast enough to be kinetically invisible in our SWV experiments. This approach was taken in all other treatments of the Marcus theory discussed herein, save for the two exceptions mentioned above.

The relative independence of all of the model parameters from square-wave pulse height is illustrated in Figures 8−10. If potential-dependent electronic tunneling[30] were significant, a systematic variation of model parameters with pulse height would be expected.

In summary, we have shown that a model combining Marcus theory and Gaussian parameter distributions is capable of successfully describing square-wave voltammograms of thin protein films. Nonlinear regression analysis onto this model allows direct estimation of electron transfer rate constants and reorganization energy from single SWV experiments at relatively large pulse height. Successful fitting of experimental data relies on the accurate representation of background current within the model.

Results indicate that reduction of $MbFe^{III}$ and oxidation of $MbFe^{II}$ in DDAB films occur with significantly different reorganization energies. This reflects real differences in solvation, bonding, and conformation near the iron heme regions of $MbFe^{III}$ and $MbFe^{II}$, a feature common to many heme proteins.

Methodology presented here promises to be generally applicable to determining Marcus electron-transfer parameters for redox proteins in thin films. Additionally, this work demonstrates the utility of some new approaches to nonlinear regression

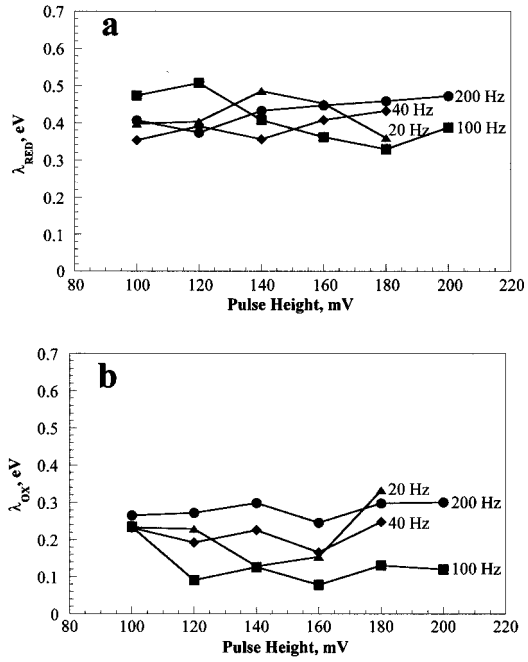

Figure 9. Influence of square-wave pulse height on mean values of λ_j from regression analyses of SWV data taken at 20−200 Hz frequency and 100−200 mV pulse height. (a) j = RED; (b) j = OX.

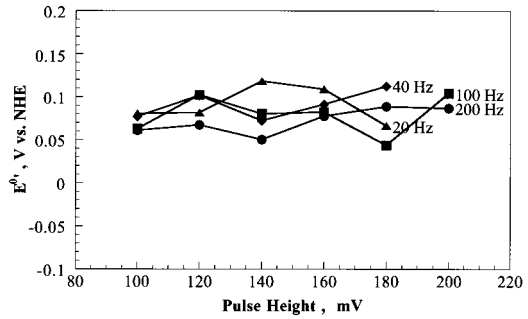

Figure 10. Influence of square-wave pulse height on mean $E^{0\prime}$ from regression analyses of SWV data taken at 20−200 Hz frequency and 100−200 mV pulse height.

analysis of complex models onto experimental data. The use of multiple linear regression coupled to nonlinear regression and the normalization and scaling of model current functions allowed for increased computational efficiency and robustness while facilitating the successful implementation of accurate background components in the model.

Acknowledgment. Financial support was provided by U.S. PHS Grant ES03154 from the National Institute of Environmental Health Sciences (NIEHS) of NIH and by the United States Department of Agriculture Grant 99-35306-7609. The authors thank Prof. William D. Chapple, University of Connecticut, for helpful discussions on Matlab programming.

Supporting Information Available: Further details on implementation of regression analysis and background modeling; one figure on modeled background and one figure on $MbFe^{III}$/$MbFe^{II}$ activation free energy. This material is available free of charge via the Internet at http://pubs.acs.org. The full Matlab *5.2* program used will be reproduced in T. Saccucci, Ph. D. Thesis, University of Connecticut, Storrs, CT, 2001.

References and Notes

(1) (a) Armstrong, F. A.; Herring, H. A.; Hirst, J. *Chem. Soc. Rev.* **1997**, *26*, 169. (b) Rusling, J. F. *Acc. Chem. Res.* **1998**, *31*, 363−369. (c) Rusling, J. F. *Prog. Colloid Polym. Sci.* **1997**, *103*, 170−180. (d) Bowden, E. F. *Interface* **1997**, 6, 40−44. (e) Rusling, J. F. In *Protein Architecture: Interfacing Molecular Assemblies and Immobilization Biotechnology*; Lvov, Y., Mohwald, H., Eds.; Marcel Dekker: New York, 2000; pp 337−354.

(2) Hirst, J.; Armstrong, F. A. *Anal. Chem.* **1998**, *70*, 5062−5071.

(3) (a) Zhang, Z.; Rusling, J. F. *Biophys. Chem.* **1997**, *63*, 133−146. (b) Nassar, A.-E. F.; Zhang, Z.; Hu, Naifei; Rusling, J. F.; Kumosinski, T. F. *J. Phys. Chem B* **1997**, *101*, 224−2231.

(4) Reeves, J. H.; Song, S.; Bowden, E. F. *Anal. Chem.* **1993**, *65*, 683−688.

(5) (a) Lvov, Y. M.; Lu, Z.; Schenkman, J. B.; Zu, Z.; Rusling, J. F. *J. Am. Chem. Soc.* **1998**, *120*, 4073−4080. (b) Clark, R. A.; Bowden, E. F. *Langmuir* **1997**, *13*, 559−565. (c) Nahir, T. M.; Bowden, E. F. *J. Electroanal. Chem.* **1996**, *410*, 9−13. (d) Nahir, T. M.; Clark, R. A.; Bowden, E. F. *Anal. Chem.* **1994**, *66*, 2595−2598.

(6) (a) Zhang, Z.; Nassar, A.-E. F.; Lu, Z.; Schenkman, J. B.; Rusling, J. F. *J. Chem. Soc., Faraday Trans.* **1997**, *93*, 1769−1774. (b) Ma, H.; Hu, N.; Rusling, J. F. *Langmuir* **2000**, *16*, 4969−4975.

(7) Albery, W. J.; Bartlett, P. J.; Wilde, C. P.; Darwent, J. R. *J. Am. Chem. Soc.* **1985**, *107*, 1854−1858.

(8) Rowe, G. K.; Carter, M. T.; Richardson, J. N.; Murray, R. W. *Langmuir* **1995**, *11*, 1797−1806.

(9) Bard, A. J.; Faulkner, L. R. *Electrochemical Methods*; Wiley: New York, 1980.

(10) Marcus, R. A.; Sutin, N. *Biochim. Biophys. Acta* **1985**, *811*, 265−322.

(11) Nassar, A.-E. F.; Zhang, Z.; Chynwat, V.; Frank, H. A.; Rusling, J. F.; Suga, K. *J. Phys. Chem.* **1995**, *99*, 11013−11017.

(12) Boussaad, S.; Tao, N. J. *J. Am. Chem. Soc.* **1999**, *121*, 4510−4515.

(13) O'Dea, J. J.; Osteryoung, J. G. *Anal. Chem.* **1993**, *65*, 3090−3097.

(14) Honeychurch, M. J. *Langmuir* **1999**, *15*, 5158−5163.

(15) (a) Weber, K.; Creager, S. E. *Anal. Chem.* **1994**, *66*, 3164−3172. (b) Tender, L.; Carter, M. T.; Murray, R. W. *Anal. Chem.* **1994**, *66*, 3173−3181. (c) Chidsey, C. E. D. *Science* **1991**, *251*, 919−922.

(16) (a) Hupp, J. T.; Weaver, M. J. *J. Phys. Chem.* **1984**, *88*, 6128−6135. (b) Hoffman, B. M.; Ratner, M. A. *J. Am. Chem. Soc.* **1987**, *109*, 6237−6243.

(17) (a) Brunori, M.; Giacometti, G. M.; Antonini, E.; Wyman, J. *J. Mol. Biol.* **1972**, *63*, 139−152. (b) Goto, Y.; Fink, A. L.. *J. Mol. Biol.* **1990**, *214*, 803−805. (c) Stigter, D.; Alonso, D. O. V.; Dill, K. A. *Proc. Natl. Acad. Sci. U.S.A.* **1991**, *88*, 4176−4180. (d) Yang, A.-S.; Honig, B. *J. Mol. Biol.* **1994**, *237*, 602−614.

(18) Rusling, J. F.; Kumosinski, T. F. *Nonlinear Computer Modeling of Chemical and Biochemical Data*; Academic Press: San Diego, 1996.

(19) (a) Levenberg, K. *Q. Appl. Math.* **1944**, *2*, 164−168. (b) Marquardt, D. *SIAM J. Appl. Math* **1963**, *11*, 431−441.

(20) Borse, G. J. *Numerical Methods With MATLAB: A Resource for Scientists and Engineers*; PWS Publishing Company: Boston, 1997.

(21) Sclereth, D. D.; Mantele, W. *Biochemistry* **1992**, *31*, 7494−7502.

(22) Some examples of recent studies: (a) Rosen, P.; Pecht, I. *Biochemistry* **1976**, *15*, 775−786. (b) Feng, Y.; Roder, H.; Englander, S. W. *Biochemistry* **1990**, *29*, 3494−3504. (c) Turner, D. 17 T.; Williams, R. J. P. *Eur. J. Biochem.* **1993**, *211*, *555*−*562*. (d) Dong, A.; Huang, P.; Caughey, *W. S. Biochemistry* **1992**, *31*, 182−189.

(23) For examples, see: (a) Blumenfeld, L. A.; Burbaev, D. S.; Davydov, R. M.; Kubrina, L. N.; Vanin, A. F.; Vilu, R. O. *Biochim. Biophy. Acta* **1975**, *379*, 512−516. (b) Ashby, G. A.; Thorneley, N. F. *Biochem. J.* **1987**, *246*, 455−465. (c) DiSpriito, A.. A.; Balney, C.; Hooper, A. *B. Eur. J. Biochem.* **1987**, *162*, 299−304. (d) Miura, S.; Ichikawa, Y. J. *Biol. Chem.* **1991**, *266*, 6252−6258. (e) Brown, E. D.; Wood, J. M. *J. Biol. Chem.* **1993**, *268*, 8972−8979.

(24) Fewnwick, C.; Marmor, S.; Govindaraju, K.; Emglish, A. M.; Wishart, J. F.; Sun, J. *J. Am. Chem. Soc.* **1994**, *116*, 3169−3170.

(25) Karas, J. L.; Lieber, C. M.; Gray, H. B. *J. Am. Chem. Soc.* **1988**, *110*, 0, 599−600.

(26) Sharp, K. A. *Biophys. J.* **1998**, *74*, 1241−1250.

(27) (a) Ortiz de Montellano, P. R., Ed. *Cytochrome P450*; Plenum: New York, 1986. (b) Schenkman, J. B.; Greim, H., Eds. *Cytochrome P450*; Springer-Verlag: Berlin, 1993.

(28) Weast, R. C., Ed. *Chemical Rubber Company Handbook of Chemistry and Physics*, *69E.*; CRC Press: Boca Raton, FL, 1988.

(29) (a) Finklea, H. O.; Hanshew, D D. D. *Am. Chem. Soc.* **1992**, *114*, 3173−3181. (b) Ravenscroft, M. S.; Finklea, H. O. *J. Phys. Chem.* **1994**, *98*, 3843−3850.

(30) (a) Forster, R. J.; Faulkner, L. R. *J. Am. Chem. Soc.* **1994**, *116*, 5444−5452. (b) Forster, R. J.; Faulkner, L. R. *J. Am. Chem. Soc.* **1994**, *116*, 5453−5461.

(31) King, B. C.; Hawkridge, F. M.; Hoffman, B. M. *J. Am. Chem. Soc.* **1992**, *114*, 10603−10608.